Two-Stage Volt-VAr Optimization of Distribution Grids with Smart Inverters and Legacy Devices

Alper Savasci, *Student Member, IEEE*, Adedoyin Inaolaji, *Student Member, IEEE*, and Sumit Paudyal, *Member, IEEE*

***Abstract*—This paper develops a two-stage Volt-VAr control (VVC) strategy coordinating the discrete controls of legacy grid devices and the operation of smart inverters (SIs) in power distribution grids with high penetration of photovoltaic (PV) generation. The first stage dispatch problem optimally coordinates the tap settings of on-load tap changers (OLTCs), on/off status of shunt capacitor banks, and SIs' active power output. The second stage incorporates the SI Volt-VAr mode, i.e., $\mathbf{Q}(\mathbf{V})$ as per IEEE-1547, and an adaptive Volt-VAr droop function, $\mathbf{Q}(\mathbf{\Delta V})$ to dispatch the SI reactive power generation. Both dispatch problems are formulated as mixed-integer linear programming (MILP) problems to maintain tractable formulations and reduce the complexity and computational burden that usually arise when solving large-scale optimal power flow (OPF) problems. The proposed two-stage strategy is tested on a modified IEEE 123-bus system considering different droop settings. The dispatch strategy augmented with $\mathbf{Q}(\mathbf{\Delta V})$ droop outperforms the model with only $\mathbf{Q}(\mathbf{V})$ droop in stabilizing the PCC voltage while resulting in less active power curtailment.**

***Index Terms*—Distribution Grids, Volt-VAr, Smart Inverters, Adaptive Control, Optimization**

I. Introduction

A. Background and Motivation

THE rapid adoption of renewable sources, encouraging regulatory actions, and favorable business models are all impetuses for the accelerated development of decarbonized and reliable energy systems [1]. This rising installation of renewable sources, however, especially in photovoltaic (PV) based distributed generation [2], creates additional challenges and opportunities in the control and management of distribution networks [3, 4]. On the one hand, the high resistance-to-reactance (R/X) ratio of distribution lines causes the feeder voltages to be significantly sensitive to active power injections in distribution networks [5], making the feeder voltages to become more vulnerable to instability due to the intermittency of PVs. On the other hand, the adoption of smart inverter (SI) technology opens new avenues in the way that voltage regulation in distribution networks can be managed. Through advanced communication and control capabilities, SIs can participate in grid-ancillary services in distribution networks [6]. Moreover, the adoption of IEEE Std. 1547-2018 [7] and IEEE Std. 1547.1-2020 [8] are standardizing and unlocking the grid-supporting functionalities and conformance of SIs interconnecting distributed energy resources (DERs) to the grid. Accordingly, distribution system operators (DSOs) can leverage the voltage regulation support from inverter-based resources (e.g., PVs) to alleviate the burden of the negative impacts of the high penetration of PVs.

Voltage regulation in the distribution network typically aims at maintaining the feeder voltage level within limits of [0.95-1.05] p.u. as specified by ANSI Standard C84.1-2011 [9]. Conventionally, Volt-VAr control (VVC) is performed by legacy grid devices such as fixed/switched capacitor banks (CBs), on-load tap changers (OLTCs) at substation transformers and step voltage regulators (SVRs). VVC is carried out in modern distribution networks as an integrated function of a distribution management system (DMS), which includes a suite of diverse control and monitoring applications. DMS-based VVC aims to achieve network-wide optimized voltage regulation by coordinating different types of VVC devices through the supervisory control and data acquisition (SCADA) [10]. VVC decisions are periodically (e.g., at every 10-15 min interval) updated to regulate voltage and reactive power through an integrated optimization algorithm.

The uptake of high renewable penetrations may require modifications in existing DMS-based VVC algorithms due to high intermittency in the output of renewable DERs [11]. Particularly, cloud transients can cause ramp up in PV generation, which scales up to 15% of its output power per minute [12], which may result in voltage fluctuation problems when the level of PV penetration exceeds 20% [13]. The conventional VVC devices can effectively regulate the slow dynamical voltage variations. However, regulation of the fast dynamical voltage variations, typically causing overvoltages, conventional VVC devices remain insufficient to tackle voltage volatility. Since LTCs and CBs are mechanical switch-based devices, their frequent operations result in wear and tear in the life cycle of conventional VVC devices. Power electronic-based fast-acting regulation devices such as STATCOMs and SVCs can also be used for over/undervoltage mitigation [13, 14]. However, new installations of such legacy volt/var control devices require initial investment by the utilities, which may not be generally intended. On the other hand, SIs provide fast and cost-effective voltage support to DSOs as they are already deployed at DER locations. Furthermore, SIs can be operated autonomously or dispatched centrally. When participating in voltage regulation autonomously, SIs can adjust active and reactive power output based on the control functions defined as Volt-VAr, i.e. $\mathbf{Q}(\mathbf{V})$; Volt-Watt, i.e. $\mathbf{P}(\mathbf{V})$; fixed-PowerFactor i.e. $\mathbf{cos}(\phi)$; PowerFactor-Watt, i.e. $\mathbf{PF}(\mathbf{P})$ as illustrated in Fig. 1.

This work is supported by National Science Foundation grant ECCS-2001732. A. Savasci, A. Inaolaji and S. Paudyal are with Department of Electrical and Computer Engineering, Florida International University. Corresponding Author: A. Savasci, Email: asava014@fiu.edu

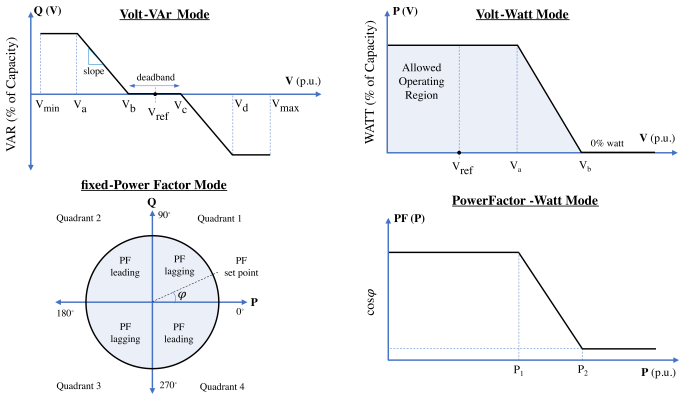

Fig. 1: Representative SI control modes.

B. Related Literature

VVC literature can be classified into coordinated and uncoordinated control approaches. Coordinated control refers to managing VVC devices collectively through a DMS-based VVC algorithm that optimizes a certain objective function, such as minimizing voltage violations and/or reducing total network losses. In contrast, uncoordinated control often covers local control strategies, which may not lead to system-wide optimum VVC. In the uncoordinated VVC schemes with no communication infrastructure, a rule-based approach is generally used for controlling each VVC device to maintain the feeder voltage within ANSI limits. Accordingly, control circuits of CBs, OLTCs, and SVRs operate autonomously with predefined settings to regulate the voltage at a specific bus or load center. In addition to the conventional VVC devices, SIs can provide local voltage regulation support by the control functions mentioned above [5, 15]. In [5], sensitivity analysis based local control strategies are analyzed for PV inverters, which can be configured with the modes of $\mathbf{Q}(\mathbf{V})$ droop, fixed reactive power, fixed power factor, and variable power factor as a function of active power generation $\mathbf{PF}(\mathbf{P})$. According to the prior analysis, authors propose a new control function combining $\mathbf{Q}(\mathbf{V})$ and $\mathbf{PF}(\mathbf{P})$ which yields $\mathbf{PF}(\mathbf{P},\mathbf{V})$. In [15], the mutual effects of autonomous control of substation OLTC and PV inverters are investigated under different local control settings of $\mathbf{Q}(\mathbf{V})$ droop, fixed-power factor and $\mathbf{PF}(\mathbf{P})$. Moreover, $\mathbf{Q}(\mathbf{V})$ droop control suggests the lowest negative impact on the substation OLTC switching operations compared with a $\mathbf{PF}(\mathbf{P})$ control. In [16], an adaptive local control strategy is proposed to improve existing $\mathbf{Q}(\mathbf{V})$ droop-based VVC support by adaptively adjusting the slope of the droop curve. The comparative results show the improvement over conventional (controls by constant parameter) and delayed droop control. Although the local VVC methods provide scalable solutions, achieving the network-wide optimal VVC without coordination might not be guaranteed. Therefore, for efficient utilization of coordinated SI functionalities that abide by the IEEE 1547, combining these SI capabilities with existing VVC schemes is unavoidable for distribution system operators (DSOs).

Accordingly, coordinated control of VVC devices with DER voltage support has been investigated in [16–20]. Coordinated VVC methods can be formulated by adopting distribution grid optimal power flow (DOPF)-based models to obtain settings of VVC devices for certain look-ahead horizons [21]. Two coordination algorithms are proposed in [17] where SIs of PV plants are operated in aggregated and autonomous mode in coordination with conventional VVC devices. SIs participate in voltage regulation by $\mathbf{Q}(\mathbf{V})$ droop-based reactive power support in autonomous mode, and a heuristic-based algorithm is carried out to dispatch LTCs, CBs, and power factor of SIs in a coordinated mode of operation. However, $\mathbf{Q}(\mathbf{V})$ droop model is not considered in an aggregated mode of operation. A hierarchical framework is proposed in [18] for coordinating the reactive power support of the PV inverters through $\mathbf{Q}(\mathbf{V})$ function. The upper hierarchy finds the optimal reactive power dispatch of PV inverters and $\mathbf{Q}(\mathbf{V})$ droop voltage intercept point by solving *LinDistFlow*-based DOPF. At the same time, local control is carried out in the lower hierarchy. However, the scalability is not shown on the practical-sized unbalanced distribution feeder. In [19], the authors propose a hierarchical dispatch mechanism considering different coordination layers for legacy devices and SIs. In addition, an adaptive slope control of $\mathbf{Q}(\mathbf{V})$ droop is proposed for the real-time operation of SIs based on local measurements. However, the exact tap changing mechanism of LTCs and $\mathbf{Q}(\mathbf{V})$ droop model of SI is not considered in the scheduling layer. In [20], a two-stage voltage regulation optimization framework is proposed considering electrical vehicles (EVs) and PV inverters. The first stage solves an optimal partitioning problem which decomposes the distribution network into multiple clusters based on sensitivity analysis, while the second stage determines the control decisions of legacy devices, EV charging/discharging, and dispatch of PV inverters by solving a MILP-based DOPF problem. The unbalanced network model is linearized, and reactive power support from PV inverters is modeled as piecewise $\mathbf{Q}(\mathbf{V})$ droop function. The overall model is solved on an hourly basis which might not be sufficient to capture the fast dynamics in PV generation.

C. Contributions

The key contributions are summarized as follows:

- A two-stage MILP-based VVC framework is proposed to dispatch legacy grid devices in coordination with the Volt-VAr support of SIs. The proposed framework, established on a linearized three-phase power flow model, incorporates the piecewise linear model of $\mathbf{Q}(\mathbf{V})$ and $\mathbf{Q}(\mathbf{\Delta V})$ droop functions of SIs and mixed-integer linear operational model of legacy devices, which significantly extends our previous studies [22, 23]. In contrast to the $\mathbf{Q}(\mathbf{V})$ droop modeling approach proposed in [20], this paper models the $\mathbf{Q}(\mathbf{V})$ droop considering each linear segment explicitly within droop breakpoints, thereby guaranteeing that the dispatch lies exactly on the droop curve and will therefore conform to IEEE 1547 [22].
- The local control strategy proposed by [24], combining Dynamic Reactive Current Control (DRCC) and Volt-VAr control modes of SIs, is reinterpreted as an operational optimization model by leveraging the derived $\mathbf{Q}(\mathbf{V})$ and

$\mathbf{Q}(\mathbf{\Delta V})$ functions. Moreover, the utilization of these droop functions within a DOPF formulation enables an adaptive dispatch model in system-wide operation, which a DMS can use to handle fast dynamic voltage events. In contrast to the scheduling layer proposed in [19], this paper makes use of the $\mathbf{Q}(\mathbf{V})$ and $\mathbf{Q}(\mathbf{\Delta V})$ functions embedded in a DOPF formulation. It can dispatch SIs reactive power output adapting to the temporal voltage deviations.

The rest of this paper is organized as follows. Section II describes the mathematical models. Section III introduces the proposed approach. In Section IV, a numerical study is executed on IEEE-123 bus test system to validate the proposed approach. Finally, the paper is concluded in Section V.

II. Mathematical Models

A. Distribution Network and Power Flow Models

A typical distribution network comprises multi-phase series and shunt components of various types. This paper considers distribution lines, buses, and OLTCs as series components, while CBs, SIs, and loads are shunt components. Each component in the network is indexed suitably and collectively represented by set notations. When indexing a bus or a shunt component connected at a bus, a single-letter subscript (e.g., i) is preferred, while a double-letter subscript (e.g., ij) is used for a branch or a series component between buses i and j. In addition, the same notational convention is followed for the electrical quantities associated with each component. The operation of the distribution network is assumed as unbalanced three-phase. Hence, the phasing of each component can have up to three phases, labeled a, b and c. The set of available phases associated with bus i and branch ij are collected within the sets $\Phi_i \subseteq \{a, b, c\}$ and $\Phi_{ij} \subseteq \{a, b, c\}$, respectively. The superscripts ϕ or ψ are used to index phasing. We also assume that the entire network is connected to an infinite bus. The connections of all components form a network topology which can be represented as a rooted tree graph by $\mathcal{G} = (\mathcal{N}, \mathcal{E})$ where $\mathcal{N}$ denotes the set of buses and $\mathcal{E}$ is the set of branches, which is formally represented $\mathcal{E} = \{(i, j)|i, j \in \mathcal{N}\}$.

Accordingly, the power flow along the network can be modeled with the well-known *LinDist3Flow* equations [25]. Decomposing the equations into real and imaginary terms of per-phase quantities yields active and reactive power balance equations in (1), where $p_j^\phi = p_j^{g,\phi} - p_j^{d,\phi}$ and $q_j^\phi = q_j^{g,\phi} - q_j^{d,\phi}$ are the net active and reactive power injections respectively, P_{jk}^ϕ and Q_{jk}^ϕ denote the active and reactive power flows outgoing from bus j while P_{ij}^ϕ and Q_{ij}^ϕ are the incoming active and reactive power flows at bus j on phase ϕ.

$$p_j^\phi = \sum_{k:j\to k} P_{jk}^\phi - \sum_{i:i\to j} P_{ij}^\phi, \ \forall j \in \mathcal{N}, \forall \phi \in \Phi_j. \tag{1a}$$

$$q_j^\phi = \sum_{k:j\to k} Q_{jk}^\phi - \sum_{i:i\to j} Q_{ij}^\phi, \quad \forall j \in \mathcal{N}, \forall \phi \in \Phi_j. \tag{1b}$$

Let $\mathcal{L} \subseteq \mathcal{E}$ be the set of distribution lines in the network. The voltage drop along the line segment can be represented as the following equation,

$$v_i^\phi = v_j^\phi - \mathbb{H}_{ij}^P P_{ij}^\phi - \mathbb{H}_{ij}^Q Q_{ij}^\phi, \quad \forall (i, j) \in \mathcal{L}, \forall \phi \in \Phi_{ij} \tag{2}$$

where $v_i^\phi = |\widetilde{V}_i^\phi|^2$ is magnitude square of the voltage phasor, $\mathbb{H}_{ij}^P$ and $\mathbb{H}_{ij}^Q$ are the modified matrices for active and reactive power flows on the line segment between buses i and j.

$$\mathbb{H}_{ij}^P = \begin{bmatrix} -2r_{ij}^{aa} & r_{ij}^{ab} - \sqrt{3}x_{ij}^{ab} & r_{ij}^{ac} + \sqrt{3}x_{ij}^{ac} \\ r_{ij}^{ba} + \sqrt{3}x_{ij}^{ba} & -2r_{ij}^{bb} & r_{ij}^{bc} - \sqrt{3}x_{ij}^{bc} \\ r_{ij}^{ca} - \sqrt{3}x_{ij}^{ca} & r_{ij}^{cb} + \sqrt{3}x_{ij}^{cb} & -2r_{ij}^{cc} \end{bmatrix} \tag{3a}$$

$$\mathbb{H}_{ij}^Q = \begin{bmatrix} -2x_{ij}^{aa} & x_{ij}^{ab} + \sqrt{3}r_{ij}^{ab} & x_{ij}^{ac} - \sqrt{3}r_{ij}^{ac} \\ x_{ij}^{ba} - \sqrt{3}r_{ij}^{ba} & -2x_{ij}^{bb} & x_{bc} + \sqrt{3}r_{ij}^{bc} \\ x_{ij}^{ca} + \sqrt{3}r_{ij}^{ca} & x_{ij}^{cb} - \sqrt{3}r_{ij}^{cb} & -2x_{ij}^{cc} \end{bmatrix} \tag{3b}$$

where resistance (r) and reactance (x) values are derived by the impedance matrix of the corresponding line configuration. Equations (1) - (3) model the network power flow in linear form.

B. LTC Model

Let $\mathcal{H} \subseteq \mathcal{E}$ denote the set of LTC branches in a distribution network. An optimization model of an LTC branch can be derived based on the single-phase branch model illustrated in Fig. 2.

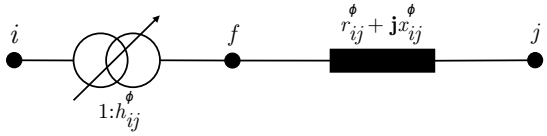

Fig. 2: Branch model with LTC.

f represents a fictitious node separating the tap changer mechanism and transformer impedance reflected to the secondary side. First, the voltage relationship of an LTC mechanism between the nodes i and f is derived as follows,

$$v_f^\phi = v_i^\phi (h_{ij}^{min,\phi} + \Delta h \cdot T_{ij}^\phi)^2 \tag{4a}$$

$$v_f^\phi = v_i^\phi (h_{ij}^{min,\phi})^2 + 2h_{ij}^{min,\phi} \Delta h \cdot v_i^\phi T_{ij}^\phi + \Delta h^2 \cdot v_i^\phi T_{ij}^{\phi 2} \tag{4b}$$

where h_{ij}^{min} is the minimum turns ratio of an auto-transformer, and Δh is the turns ratio step size per tap change, which are physical parameters, while T_{ij}^ϕ denotes the integer tap value as a manipulated variable. The novelty in this subsection is the derivation of a valid linearized expression for (4b) by reformulation techniques for the nonlinear terms. Defining new variables $A_{ij}^\phi := v_i^\phi T_{ij}^\phi$ and $B_{ij}^\phi := v_i^\phi (T_{ij}^\phi)^2$, (4b) yields the following linear form.

$$v_f^\phi = v_i^\phi (h_{ij}^{min,\phi})^2 + 2h_{ij}^{min,\phi} \Delta h \cdot A_{ij}^\phi + \Delta h^2 \cdot B_{ij}^\phi. \tag{4c}$$

Using the binary expansion technique, integer tap values can be linearly represented as

$$T_{ij}^\phi = \sum_{n=0}^{K_{ij}^\phi} 2^n b_{ij,n}^\phi \tag{4d}$$

where $b^{\phi}_{ij,n}$ is a binary variable corresponding to n-th digit. Suppose that N^{ϕ}_{ij} is the total number of tap values, then let $K^{\phi}_{ij} = log_2(N^{\phi}_{ij} - 1)$ be the number of digits required to represent the integer tap values. Multiplying both sides of (4d) by v^{ϕ}_i yields (4e).

$$v^{\phi}_i T^{\phi}_{ij} = \sum_{n=0}^{K^{\phi}_{ij}} 2^n b^{\phi}_{ij,n} v^{\phi}_i. \tag{4e}$$

Note that the right-hand side of (4e) is composed of a sum of bilinear terms which can be reformulated by introducing a new auxiliary variable $w^{\phi}_{ij,n} := b^{\phi}_{ij,n} v^{\phi}_i$ and adding two extra constraints for each digit as follows,

$$A^{\phi}_{ij} := \sum_{n=0}^{K^{\phi}_{ij}} 2^n w^{\phi}_{ij,n}. \tag{4f}$$

$$b_{ij,n}\underline{v^{\phi}_i} \le w^{\phi}_{ij,n} \le b^{\phi}_{ij,n}\overline{v^{\phi}_i}. \tag{4g}$$

$$-\overline{v^{\phi}_i}(1 - b^{\phi}_{ij,n}) \le v^{\phi}_i - w^{\phi}_{ij,n} \le \overline{v^{\phi}_i}(1 - b^{\phi}_{ij,n}). \tag{4h}$$

Reformulation of the second nonlinear term, $v^{\phi}_i (T^{\phi}_{ij})^2$, in (4b) can also be derived with a similar procedure. Taking the square of both sides of (4d) yields(4i).

$$\left(T^{\phi}_{ij}\right)^2 = \left(\sum_{n=0}^{K^{\phi}_{ij}} 2^n b^{\phi}_{ij,n}\right)^2. \tag{4i}$$

Next, we leverage on a square of a sum identity as (4j), where m and n are digit indices.

$$\left(\sum_n a_n\right)^2 = \sum_n a_n^2 + 2\sum_{n<m} a_n a_m \tag{4j}$$

The squared expression on the right-hand side of (4i) can then be expanded as follows

$$\left(T^{\phi}_{ij}\right)^2 = \sum_{n=0}^{K^{\phi}_{ij}} (2^n b^{\phi}_{ij,n})^2 + 2\sum_{n<m}^{K^{\phi}_{ij}} (2^n b^{\phi}_{ij,n})(2^m b^{\phi}_{ij,m}) \tag{4k}$$

$$= \sum_{n=0}^{K^{\phi}_{ij}} 4^n b^{\phi}_{ij,n} + 2\sum_{n<m}^{K^{\phi}_{ij}} (2^{n+m}) b^{\phi}_{ij,n} b^{\phi}_{ij,m}. \tag{4l}$$

Note that the square of a binary number is itself. The bilinear binary product terms appearing in the second summation of eq. (4l) can be replaced by an auxiliary variable $z^{\phi}_{ij,nm} := b^{\phi}_{ij,n} b^{\phi}_{ij,m}$, which is equivalent to logical AND operation for the binary variables which can be reformulated as follows

$$z^{\phi}_{ij,nm} \ge b^{\phi}_{ij,n} + b^{\phi}_{ij,m} - 1 \tag{4m}$$

$$z^{\phi}_{ij,nm} \le b^{\phi}_{ij,n} \tag{4n}$$

$$z^{\phi}_{ij,nm} \le b^{\phi}_{ij,m}. \tag{4o}$$

By multiplying both sides of (4l) by v^{ϕ}_i, the second nonlinear term in (4b) is derived as

$$v^{\phi}_i (T^{\phi}_{ij})^2 = \sum_{n=0}^{K^{\phi}_{ij}} 4^n b^{\phi}_{ij,n} v^{\phi}_i + 2\sum_{n<m}^{K^{\phi}_{ij}} (2^{n+m}) z^{\phi}_{ij,nm} v^{\phi}_i. \tag{4p}$$

The auxiliary variable, $w^{\phi}_{ij,n} := b^{\phi}_{ij,n} v^{\phi}_i$, has already been defined previously and can be used for the first part of the expression (4p). A new auxiliary variable $y^{\phi}_{ij,nm} := z^{\phi}_{ij,nm} v^{\phi}_i$ is introduced for the bilinear term in the second part, which yields the following expression,

$$B^{\phi}_{ij} := \sum_{n=0}^{K^{\phi}_{ij}} 4^n w^{\phi}_{ij,n} + 2\sum_{n<m}^{K^{\phi}_{ij}} (2^{n+m}) y^{\phi}_{ij,nm} \tag{4q}$$

$$z_{ij,nm}\underline{v^{\phi}_i} \le y^{\phi}_{ij,nm} \le z^{\phi}_{ij,nm}\overline{v^{\phi}_i} \tag{4r}$$

$$-\overline{v^{\phi}_i}(1 - z^{\phi}_{ij,nm}) \le v^{\phi}_i - y^{\phi}_{ij,nm} \le \overline{v^{\phi}_i}(1 - z^{\phi}_{ij,n}). \tag{4s}$$

Finally, the nonlinear LTC mechanism voltage relationship is reformulated in mixed-integer linear form, which is more amenable to efficient mathematical programming solvers.

Compactly,

$$\left.\begin{matrix}(4c), (4f) - (4h), (4m) - (4o) \\ (4q) - (4s)\end{matrix}\right\}, \forall (i,j) \in \mathcal{H},\ \phi \in \Phi^{\mathcal{H}}_{ij} \tag{5}$$

forms the LTC model.

C. Capacitor Bank Model

Let $\mathcal{C} \subseteq \mathcal{N}$ denote the set of buses to which CBs are connected. The total reactive power support from a capacitor bank connected at node j can be modeled by the following equation,

$$q^{\phi,c}_j = \sum_{n=1}^{N_c} u^{\phi,c}_{jn} \cdot Q^{\phi,c}_{jn} \quad \forall i \in \mathcal{C},\ \phi \in \Phi^{\mathcal{C}}_i \tag{6}$$

where $u^{\phi,c}_{jn} = \{0,1\}$ is a binary variable representing the switching off/on operation of the n-th capacitor unit, $Q^{\phi,c}_{jn}$ represents the rating of the corresponding unit, and N_c is the total number of the capacitor unit.

D. SI Operational Model

A SI is a power electronic device that converts DC to AC and interfaces solar, wind, energy storage, and electric vehicles to the distribution grid. In this study, the term SI is used for a PV-based inverter system connected to the grid at the point of common coupling (PCC). Through a set of advanced control functions, SI can contribute to voltage regulation by modulating its active and reactive power output as a function of the voltage measured at PCC [7, 26]. A typical power output capability curve of an SI can be represented in Fig. 3. To fully utilize its capability of injecting (capacitive) and absorbing (inductive) reactive power, the SI is oversized such that its apparent power rating is designed to be greater than its active power rating. In this way, the SI can still generate reactive power even if the active power output is dispatched at its maximum capacity.

In terms of multi-phase modeling, let $p^{g,\phi}_i$ and $q^{g,\phi}_i$ denote the controllable power output of an SI connected at bus i and phase ϕ, then (7) typically defines the relation between active and reactive power outputs with the apparent power rating of SI as

$$\sqrt{(p^{g,\phi}_i)^2 + (q^{g,\phi}_i)^2} \le S^{\phi}_{rating,i}, \quad \forall i \in \mathcal{N}_{\text{PV}},\ \forall \phi \in \Phi^{\text{PV}}_i \tag{7}$$

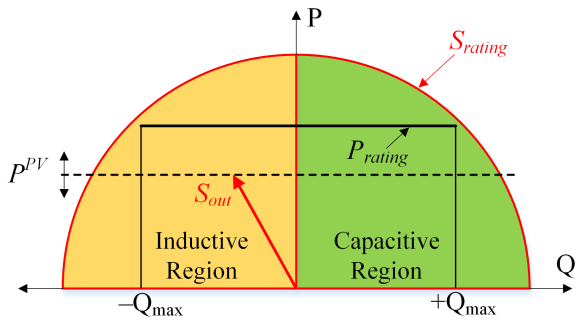

Fig. 3: Power output capability of SIs.

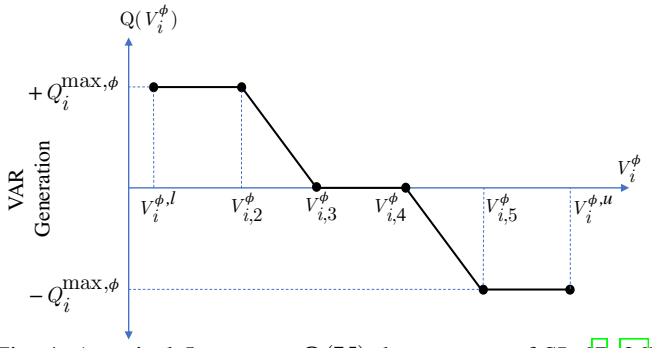

Fig. 4: A typical 5-segment $\mathbf{Q}(\mathbf{V})$ droop curve of SIs [7, 26].

where the sets $\mathcal{N}_{\text{PV}}$ and Φ_i^{PV} represent the set of SI connected buses and corresponding phase set, respectively. The direct use of (7) is not possible in a linear optimization model when both the active power and reactive power are decision variables. Therefore, [27] proposes to linearly approximate (7) by making use of a 32-vertex polygon ($k = 16$) and defining a polyhedral norm as,

$$\begin{aligned} -S^{\phi}_{rating,i} \leq \cos(l\gamma)\ p_i^{g,\phi} + \sin(l\gamma)\ q_i^{g,\phi} \leq S^{\phi}_{rating,i} \\ \gamma = \frac{\pi}{k}, \quad l = 1, \cdots, k, \quad \forall i \in \mathcal{N}_{\text{PV}},\ \forall \phi \in \Phi_i^{\text{PV}}. \end{aligned} \tag{8}$$

Given that $P_{rating,i}$ and $Q_i^{\max,\phi}$ denote the active and reactive power rating respectively of SI, the following box constraints ensure the active and reactive power capabilities.

$$0 \leq p_i^{g,\phi} \leq P_{rating,i}, \quad \forall i \in \mathcal{N}_{\text{PV}},\ \forall \phi \in \Phi_i^{\text{PV}}. \tag{9}$$

$$-Q_i^{\max,\phi} \leq q_i^{g,\phi} \leq Q_i^{\max,\phi}, \quad \forall i \in \mathcal{N}_{\text{PV}},\ \forall \phi \in \Phi_i^{\text{PV}}. \tag{10}$$

E. Modeling of Volt-VAr Droop Curve

The autonomous operation of DER units is generally carried out utilizing droop-based control methods in which active or reactive power outputs are adjusted based on a specific mathematical function. Volt-VAr curve/droop is one function that allows SIs to participate in voltage regulation by providing reactive power support as a function of voltage at the PCC. Fig. 4 depicts a typical $\mathbf{Q}(\mathbf{V})$ droop with five piecewise linear segments. The range of each segment determines how SI modulates its reactive power output. The SI neither absorbs nor injects reactive power when the voltage stays within the nominal voltage range $[V_{i,3}^{\phi}, V_{i,4}^{\phi}]$, called deadband. When the voltage decreases into $[V_{i,2}^{\phi}, V_{i,3}^{\phi}]$, SI modulates its reactive power output by a constant slope in capacitive mode. However, smaller voltage values within $[V_i^{\phi,l}, V_{i,2}^{\phi}]$ drives SI to the capacitive saturation range. Similarly, in the range of $[V_{i,4}^{\phi}, V_{i,5}^{\phi}]$, inductive mode is active with the slope while SI stays at inductive saturation in $[V_{i,5}^{\phi}, V_i^{\phi,u}]$. Depending on the configuration of the breakpoints, the available operating range of the voltage is partitioned into multiple segments, which define the reactive power control actions of the SIs.

It is necessary to obtain an analytical model of the $\mathbf{Q}(\mathbf{V})$ droop curve of SIs in order to integrate it into the DOPF formulation. Thus, [22] proposes an analytical way of modeling $\mathbf{Q}(\mathbf{V})$ droop curve through a piecewise modeling approach. The mathematical representation of $\mathbf{Q}(\mathbf{V})$ droop curve can be written as the following piecewise function having five segments,

$$Q_i(V_i^{\phi}) = \begin{cases} +Q_i^{\max,\phi}, & V_i^{\phi,l} \leq V_i^{\phi} \leq V_{i,2}^{\phi} \\ \frac{-Q_i^{\max,\phi}}{V_{i,3}^{\phi} - V_{i,2}^{\phi}} V_i^{\phi} + \frac{Q_i^{\max,\phi} V_{i,3}^{\phi}}{V_{i,3}^{\phi} - V_{i,2}^{\phi}}, & V_{i,2}^{\phi} < V_i^{\phi} \leq V_{i,3}^{\phi} \\ 0, & V_{i,3}^{\phi} < V_i^{\phi} \leq V_{i,4}^{\phi} \\ \frac{-Q_i^{\max,\phi}}{V_{i,5}^{\phi} - V_{i,4}^{\phi}} V_i^{\phi} + \frac{Q_i^{\max,\phi} V_{i,4}^{\phi}}{V_{i,5}^{\phi} - V_{i,4}^{\phi}}, & V_{i,4}^{\phi} < V_i^{\phi} \leq V_{i,5}^{\phi} \\ -Q_i^{\max,\phi}, & V_{i,5}^{\phi} < V_i^{\phi} \leq V_i^{\phi,u} \end{cases} \tag{11}$$

where $V_{i,2}^{\phi}$ through $V_{i,5}^{\phi}$ are the break points of voltage V_i^{ϕ} whose lower and upper bounds are given as $V_i^{\phi,l}$ and $V_i^{\phi,u}$ respectively.

The value of the node voltage V_i^{ϕ} determines the segment to be activated through the use of binary variables, i.e., $\delta_{i,1}, \ldots, \delta_{i,5} \in \{0, 1\}$, and $Q_i(V_i^{\phi})$ function can be collectively written as,

$$\begin{aligned} Q_i(V_i^{\phi}) = \ & \delta_{i,1}^{\phi} \left(+Q_i^{\max,\phi} \right) \\ & + \delta_{i,2}^{\phi} \left(\frac{-Q_i^{\max,\phi}}{V_{i,3}^{\phi} - V_{i,2}^{\phi}} V_i^{\phi} + \frac{Q_i^{\max,\phi} V_{i,3}^{\phi}}{V_{i,3}^{\phi} - V_{i,2}^{\phi}} \right) \\ & + \delta_{i,3}^{\phi} (0) \\ & + \delta_{i,4}^{\phi} \left(\frac{-Q_i^{\max,\phi}}{V_{i,5}^{\phi} - V_{i,4}^{\phi}} V_i^{\phi} + \frac{Q_i^{\max,\phi} V_{i,4}^{\phi}}{V_{i,5}^{\phi} - V_{i,4}^{\phi}} \right) \\ & + \delta_{i,5}^{\phi} \left(-Q_i^{\max,\phi} \right) \end{aligned} \tag{12}$$

where only one binary variable is activated to choose one segment of $Q_i(V_i)$, while disabling the other segments. This condition is enforced by the following logical constraint,

$$\sum_{m=1}^{5} \delta_{i,m}^{\phi} = 1. \tag{13}$$

Utilizing big-M modelling approach, the voltage ranges of each segment, defined by break points of $Q_i(V_i^{\phi})$ in (11), can be combined with the binary variables through the following set of inequalities,

$$\left.\begin{aligned}
&-(1-\delta_{i,1}^{\phi})\,M + V_i^{\phi,l} \le V_i^{\phi} \le V_{i,2}^{\phi} + (1-\delta_{i,1}^{\phi})\,M \\
&-(1-\delta_{i,2}^{\phi})\,M + V_{i,2}^{\phi} \le V_i^{\phi} \le V_{i,3}^{\phi} + (1-\delta_{i,2}^{\phi})\,M \\
&-(1-\delta_{i,3}^{\phi})\,M + V_{i,3}^{\phi} \le V_i^{\phi} \le V_{i,4}^{\phi} + (1-\delta_{i,3}^{\phi})\,M \\
&-(1-\delta_{i,4}^{\phi})\,M + V_{i,4}^{\phi} \le V_i^{\phi} \le V_{i,5}^{\phi} + (1-\delta_{i,4}^{\phi})\,M \\
&-(1-\delta_{i,5}^{\phi})\,M + V_{i,5}^{\phi} \le V_i^{\phi} \le V_i^{\phi,u} + (1-\delta_{i,5}^{\phi})\,M
\end{aligned}\right\} \quad (14)$$

where M is a sufficiently large disjunctive parameter, which can be selected as $V_i^{\phi,u}$.

The piecewise nature of the $Q_i(V_i^{\phi})$ droop curve can be exactly modelled by the set of equations given by (12)-(14). However, the bilinear terms occurring in (12), which are the products of binary variable δ_i and continuous variable V_i, making the overall analytical droop model nonlinear. These particularly occur at the 2^{nd} and 4^{th} segments where the $Q_i(V_i^{\phi})$ curve has slopes. Hence, we apply an exact linearization method to the bilinear terms in (12). Consider two new variables $W_{i,2}^{\phi} := \delta_{i,2}^{\phi}\, V_i^{\phi}$ and $W_{i,4}^{\phi} := \delta_{i,4}^{\phi}\, V_i^{\phi}$. Then, (12) is reformulated as following,

$$\begin{aligned}
Q(V_i^{\phi}) = {} & \delta_{i,1}^{\phi}\left(Q_i^{\max,\phi}\right) \\
& + W_{i,2}^{\phi}\left(\frac{-Q_i^{\max,\phi}}{V_{i,3}^{\phi} - V_{i,2}^{\phi}}\right) + \delta_{i,2}^{\phi}\left(\frac{Q_i^{\max,\phi}\, V_{i,3}^{\phi}}{V_{i,3}^{\phi} - V_{i,2}^{\phi}}\right) \\
& + \delta_{i,3}^{\phi}\,(0) \\
& + W_{i,4}^{\phi}\left(\frac{-Q_i^{\max,\phi}}{V_{i,5}^{\phi} - V_{i,4}^{\phi}}\right) + \delta_{i,4}^{\phi}\left(\frac{Q_i^{\max,\phi}\, V_{i,4}^{\phi}}{V_{i,5}^{\phi} - V_{i,4}^{\phi}}\right) \\
& + \delta_{i,5}^{\phi}\left(-Q_i^{\max,\phi}\right)
\end{aligned} \quad (15)$$

where new variables are coupled with existing segment bounds with a modified set of inequalities as,

$$\left.\begin{aligned}
&-(1-\delta_{i,1}^{\phi})\,M + V_i^{\phi,l} \le V_i^{\phi} \le V_{i,2}^{\phi} + (1-\delta_{i,1}^{\phi})\,M \\
&-M\,(1-\delta_{i,2}^{\phi}) \le V_i^{\phi} - W_{i,2}^{\phi} \le (1-\delta_{i,2}^{\phi})\,M \\
&V_{i,2}^{\phi}\,\delta_{i,2}^{\phi} \le W_{i,2}^{\phi} \le V_{i,3}^{\phi}\,\delta_{i,2}^{\phi} \\
&-(1-\delta_{i,3}^{\phi})\,M + V_{i,3}^{\phi} \le V_i^{\phi} \le V_{i,4}^{\phi} + (1-\delta_{i,3}^{\phi})\,M \\
&-M\,(1-\delta_{i,4}^{\phi}) \le V_i^{\phi} - W_{i,4}^{\phi} \le (1-\delta_{i,4}^{\phi})\,M \\
&V_{i,4}^{\phi}\,\delta_{i,4}^{\phi} \le W_{i,4}^{\phi} \le V_{i,5}^{\phi}\,\delta_{i,4}^{\phi} \\
&-(1-\delta_{i,5}^{\phi})\,M + V_{i,5}^{\phi} \le V_i^{\phi} \le V_i^{\phi,u} + (1-\delta_{i,5}^{\phi})\,M
\end{aligned}\right\} \quad (16)$$

An integer-linear form of an analytical model of $\mathbf{Q}(\mathbf{V})$ droop curve can thus be obtained by the equations (17).

$$\{(13), (15), (16)\} \quad \forall i \in \mathcal{N}_{\text{PV}},\ \phi \in \Phi_i^{\text{PV}}. \quad (17)$$

F. Adaptive Volt-VAr Droop Function

Due to the intermittent nature of PV generation, time-varying and rapid voltage fluctuations can occur within a day, which results in power quality issues. In order to improve the power quality and stabilize the voltage at PCC, Dynamic-Reactive Current Control (DRCC) method has been recommended for SIs [26]. The DRCC method is based on the voltage difference (ΔV) between the present voltage and a voltage reference, specified as a percent change or deviation from the reference voltage. The reference voltage can be chosen as the average voltage calculated by the voltage samples within the moving window defined over the previous time intervals.

The local DRCC and Volt-VAr droop, $\mathbf{Q}(\mathbf{V})$, functionalities have further been combined in [24], and called "Volt-VAr with Adaptive Control". Through the adaptive capability, the generated reactive power is proportional to the magnitude of temporal voltage deviations so that the PCC voltage deviations can be compensated against the temporal cloud-induced voltage fluctuations. Fig. 5 shows the conceptual block diagram of the modified approach where we combine adaptive and normal Volt-VAr functions.

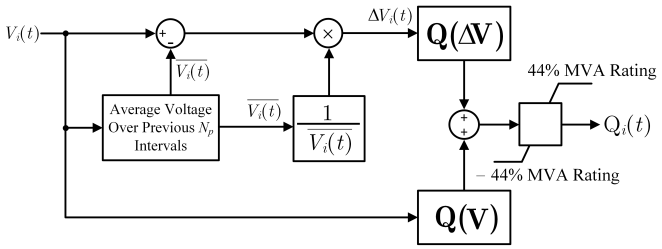

Fig. 5: Modified control strategy [24].

The average voltage, $\overline{V_i^{\phi}(t)}$, calculated at time interval t over a time window is defined as

$$\overline{V_i^{\phi}(t)} = \frac{1}{N_p}\sum_{\tau=1}^{N_p} V_i^{\phi}(t-\tau) \quad (18)$$

where N_p is the averaging window size. Instead of using only voltage difference, we further modify the proposed approach as shown in Fig. 5, by adding relative voltage difference functionality defined in (19).The voltage change at present time interval $\Delta V_i(t)$ at bus i is calculated as follows

$$\Delta V_i^{\phi} = \left[\frac{V_i(t)^{\phi} - \overline{V_i(t)^{\phi}}}{\overline{V_i(t)^{\phi}}}\right] \cdot 100\% \quad (19)$$

where $V_i(t)$ can be selected as a control variable in optimal/adaptive control applications and the time index t is dropped for the brevity in the following formulations.

In order to utilize the modified "Volt-VAr with Adaptive Control" approach inside an optimization framework, the mathematical model of adaptive droop, $\mathbf{Q}(\mathbf{\Delta V})$, is required to be derived and merged with OPF formulation. Unlike the $\mathbf{Q}(\mathbf{V})$ droop, where the reactive power output is a function of the voltage magnitude, the adaptive Volt-VAr droop function is denoted by $\mathbf{Q}(\mathbf{\Delta V})$, which is a function of voltage magnitude deviation as shown in Fig. 6. Similar to the $\mathbf{Q}(\mathbf{V})$ droop, $\mathbf{Q}(\mathbf{\Delta V})$ droop can be defined as a piecewise linear function with suitable breakpoints.

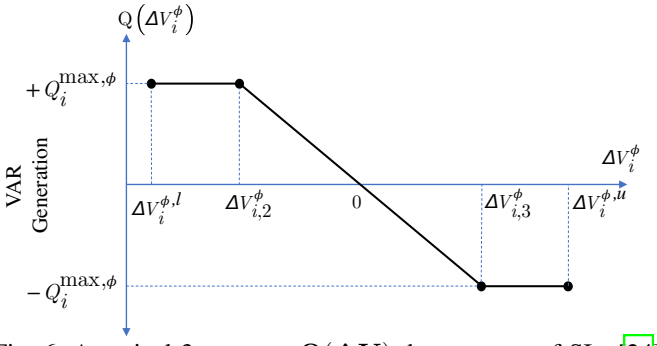

Fig. 6: A typical 3-segment $\mathbf{Q}(\mathbf{\Delta V})$ droop curve of SIs. [24]

The $\mathbf{Q}(\mathbf{\Delta V})$ of SIs is modeled by applying the same procedure of mixed-integer modeling of normal Volt-VAr droop $\mathbf{Q}(\mathbf{V})$ detailed in Section II.E. The mathematical representation of $\mathbf{Q}(\mathbf{\Delta V})$ droop curve can be given as the following piecewise function in (20).

$$Q_i(\Delta V_i^\phi) = \begin{cases} +Q_i^{\max,\phi}, & \Delta V_i^{\phi,l} \le \Delta V_i^\phi \le \Delta V_{i,2}^\phi \\ \frac{-2Q_i^{\max,\phi}}{\Delta V_{i,3}^\phi - \Delta V_{i,2}^\phi}\,\Delta V_i^\phi, & \Delta V_{i,2}^\phi < \Delta V_i^\phi \le \Delta V_{i,3}^\phi \\ -Q_i^{\max,\phi}, & \Delta V_{i,3}^\phi < \Delta V_i^\phi \le \Delta V_i^{\phi,u} \end{cases} \tag{20}$$

Combining all intervals using binary indicator variables, $\alpha_{i,m}$, it yields the following function representation,

$$\begin{aligned} Q_i(\Delta V_i^\phi) = \; & \alpha_{i,1}^\phi\,(+Q_i^{\max,\phi}) \\ & + \alpha_{i,2}^\phi \left(\frac{-2Q_i^{\max,\phi}}{\Delta V_{i,3}^\phi - \Delta V_{i,2}^\phi}\,\Delta V_i^\phi\right) \\ & + \alpha_{i,3}^\phi\,(-Q_i^{\max,\phi}). \end{aligned} \tag{21}$$

Defining a new variable $Z_{i,2}^\phi := \alpha_{i,2}^\phi\,\Delta V_i^\phi$. Then, (21) is reformulated linearly as following,

$$\begin{aligned} Q_i(\Delta V_i^\phi) = \; & \alpha_{i,1}^\phi \left(+Q_i^{\max,\phi}\right) \\ & + Z_{i,2}^\phi \left(\frac{-2Q_i^{\max,\phi}}{\Delta V_{i,3}^\phi - \Delta V_{i,2}^\phi}\right) \\ & + \alpha_{i,3}^\phi \left(-Q_i^{\max,\phi}\right) \end{aligned} \tag{22}$$

$$\left.\begin{gathered} -(1-\alpha_{i,1}^\phi)\,M + \Delta V_i^{\phi,l} \le \Delta V_i^\phi \le \Delta V_{i,2}^\phi + (1-\alpha_{i,1}^\phi)\,M \\ -M\,(1-\alpha_{i,2}^\phi) \le \Delta V_i - Z_{i,2}^\phi \le (1-\alpha_{i,2}^\phi)\,M \\ \Delta V_{i,2}^\phi\,\alpha_{i,2}^\phi \le Z_{i,2}^\phi \le \Delta V_{i,3}^\phi\,\alpha_{i,2}^\phi \\ -(1-\alpha_{i,3}^\phi)\,M + \Delta V_{i,3}^\phi \le \Delta V_i^\phi \le \Delta V_i^{\phi,u} + (1-\alpha_{i,3}^\phi)\,M \end{gathered}\right\} \tag{23}$$

$$\sum_{m=1}^{3} \alpha_{i,m}^\phi = 1. \tag{24}$$

The analytical model of integer-linear $\mathbf{Q}(\mathbf{\Delta V})$ droop curve representation can be given as

$$\{\ (22), (23), (24)\ \} \quad \forall i \in \mathcal{N}_{\text{PV}},\ \phi \in \Phi_i^{\text{PV}}. \tag{25}$$

G. Base Distribution Grid OPF Model

The developed operational models of different distribution system equipment can be coupled with a power flow model to optimize a grid objective such as total line loss, curtailment, or feeder voltage profile.

A DOPF model can be formulated as a mixed-integer linear program (MILP). In this study, the DOPF1 model is given as follows,

DOPF1 :

$$\begin{aligned} \text{Min} \quad OF_1 = \; & \xi_1 \sum_{i\in\mathcal{N}^{\text{PV}}} \sum_{\phi\in\Phi_i^{\text{PV}}} (\widehat{P_{pv}}_{i,t} - p_{i,t}^{g,\phi}) \\ & + \xi_2 \sum_{i\in\mathcal{N}\setminus\mathcal{N}'} \sum_{\phi\in\Phi_i} |v_{i,t}^\phi - v_{ref}| \\ & + \xi_3 \sum_{(i,j)\in\mathcal{H}} \sum_{\phi\in\Phi_{ij}} |T_{ij,t}^\phi - T_{ij,t-1}^\phi| \\ & + \xi_4 \sum_{i\in\mathcal{C}} \sum_{\phi\in\Phi_{ij}^c} |u_{i,t}^{\phi,c} - u_{i,t-1}^{\phi,c}| \end{aligned} \tag{26a}$$

$$\text{Subject to :}$$

$$(1), (2)-(3), (5), (6), (8)-(10) \tag{26b}$$

$$\left.\begin{gathered} p_j^{g,\phi} \in [p_j^{g,l},\, p_j^{g,u}] \\ q_j^{g,\phi} \in [q_j^{g,l},\, q_j^{g,u}] \end{gathered}\right\} \forall j \in \mathcal{N}' \setminus \mathcal{N}_{\text{PV}}, \forall \phi \in \Phi_j \tag{26c}$$

$$v_j^\phi \in [v_j^l,\, v_j^u], \qquad \forall j \in \mathcal{N}', \forall \phi \in \Phi_j. \tag{26d}$$

The OF_1 comprises four objective terms, which are total PV curtailment, total voltage deviation from the reference voltage value, total absolute tap position and CB switching deviations from the previous dispatch interval, $\xi_1, \xi_2, \xi_3, \xi_4$ are the weights used for maintaining the sufficient effect of each corresponding term. The function of DOPF1 is to minimize the legacy devices switching operations while minimizing the power flow from the upstream network by utilizing the PV generation as much as possible.

H. First Order Voltage Approximation

The key challenge associated with incorporating the analytical SI droop models with the underlying three-phase power flow model (*LinDist3Flow*) is that the droop curves use the first order of voltage magnitude V_i^ϕ and ΔV_i^ϕ. In contrast, the *LinDist3Flow* model uses the square of voltage magnitude, i.e., v_i^ϕ. It is therefore imperative to include the exact relationship of $v_i^\phi = (V_i^\phi)^2$ when using *LinDist3Flow*. However, enforcing this quadratic relationship as an exact constraint would result in a nonlinear DOPF, thereby defeating the purpose of using a linearized power flow model. Thus, such a relationship can be reformulated as a linear or mixed-integer linear constraint to conform with the modeling structure of the *LinDist3Flow*-based DOPF model.

Although other approximation or linearization methods can be applied to the quadratic voltage relationship, we prefer to use Taylor Series Expansion (TSE) as its accuracy has been found sufficient in [22]. The quadratic voltage relationship can be approximated by TSE around an operating point V_o^ϕ as follows,

$$v_i^{\phi} = (V_o^{\phi})^2 + 2V_o^{\phi}(V_i^{\phi} - V_o^{\phi}) + (V_i^{\phi} - V_o^{\phi})^2, \quad \forall i \in \mathcal{N}_{\text{PV}}, \forall \phi \in \Phi_i^{\text{PV}} \quad (27a)$$

where $V_o^{\phi} \in [V_i^l, V_i^u]$. If the quadratic term in (27a) is ignored, it can be approximated as the following linear model,

$$\langle (V_i^{\phi})^2 \rangle^{TSE} \equiv V_o^{\phi 2} + 2V_o^{\phi}(V_i^{\phi} - V_o^{\phi}), \quad \forall i \in \mathcal{N}_{\text{PV}}, \forall \phi \in \Phi_i^{\text{PV}} \quad (27b)$$

where the elimination of quadratic term leads to an error whose value depends on the choice of parameter V_o^{ϕ}.

I. Volt-VAr Droop Integrated DOPF Models

Based on the modeled droop curves, it is possible to formulate two variants of DOPF models for coordinating the legacy devices with the Volt-VAr function of SIs. The first DOPF model includes the regular $\mathbf{Q}(\mathbf{V})$ droop function, which is called DOPF2-QV.

DOPF2 – QV :

$$\text{Min} \quad OF_2 = \sum_{i \in \mathcal{N}^{\text{PV}}} \sum_{\phi \in \Phi_i^{\text{PV}}} (\widehat{P_{pv}}_{i,t} - p_{i,t}^{g,\phi}) \quad (28a)$$

Subject to :

$$(1), (2) - (3), (5), (6), (8) - (10) \quad (28b)$$

$$\text{First-order Voltage Approximation : (27b)} \quad (28c)$$

$$\text{SI } \mathbf{Q}(\mathbf{V}) \text{ Droop Model : (17)} \quad (28d)$$

$$q_j^{g,\phi} = \mathbf{Q}(V_j^{\phi}) \quad \forall j \in \mathcal{N}_{\text{PV}}, \forall \phi \in \Phi_j^{\text{PV}} \quad (28e)$$

$$(26c), (26d). \quad (28f)$$

The second DOPF model includes the $\mathbf{Q}(\mathbf{\Delta V})$ droop function model as an addition then referred as DOPF2-QΔV model as follows

DOPF2 – Q$\mathbf{\Delta V}$:

$$\text{Min} \quad OF_2 = \sum_{i \in \mathcal{N}^{\text{PV}}} \sum_{\phi \in \Phi_i^{\text{PV}}} (\widehat{P_{pv}}_{i,t} - p_{i,t}^{g,\phi}) \quad (29a)$$

Subject to :

$$(1), (2) - (3), (5), (6), (8) - (10) \quad (29b)$$

$$\text{First-order Voltage Approximation : (27b)} \quad (29c)$$

$$\text{SI } \mathbf{Q}(\mathbf{V}) \text{ Droop Model : (17)} \quad (29d)$$

$$\text{SI } \mathbf{Q}(\mathbf{\Delta V}) \text{ Droop Model : (25)} \quad (29e)$$

$$q_j^{g,\phi} = \mathbf{Q}(V_j^{\phi}) + \mathbf{Q}(\Delta V_j^{\phi}) \quad \forall j \in \mathcal{N}_{\text{PV}}, \forall \phi \in \Phi_j^{\text{PV}} \quad (29f)$$

$$(26c), (26d). \quad (29g)$$

III. Proposed Coordination Approach

This section presents the proposed two optimization frameworks for coordinated dispatch of the VVC devices. Both frameworks make use of the two-stage optimization approach as depicted in Fig. 7, where two optimization models are solved at each stage in a nested-loop structure. In the first stage, the DOPF1 model is run to find the dispatch decisions for the tap positions of LTCs, and the on/off status of CBs considering the amount of active power generation of SIs with respect to the available PV power capacity, which is provided as a forecasted data. Then, the DOPF2 model is run in the second stage, while the discrete decisions for LTCs and CBs are fixed to the solution obtained in the first stage.

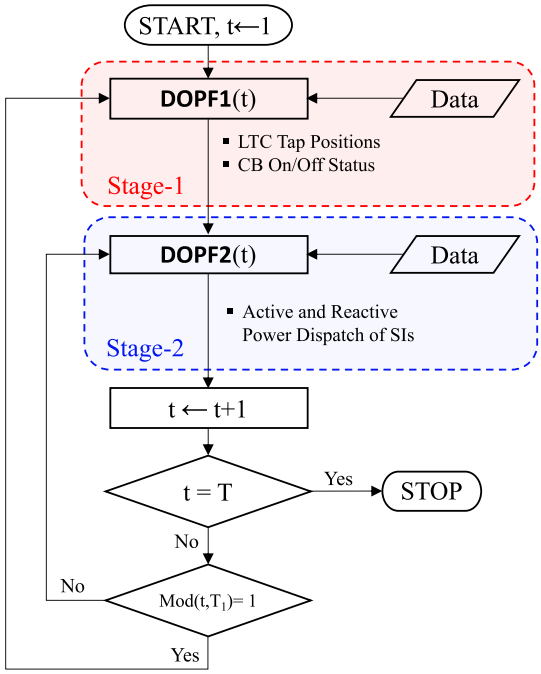

Fig. 7: Two-stage optimization procedure.

The execution of DOPF1 and DOPF2 models are allocated to coarse and finer timescales, respectively, considering the operational characteristics of the VVC devices. A representative N-interval dispatch window of DOPF1 and DOPF2 is illustrated in Fig. 8.

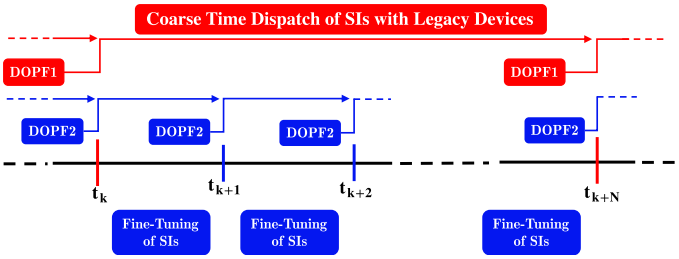

Fig. 8: Timing diagram of two-timescale operation.

Conforming to this timing diagram, the dispatch period of DOPF1 covers N-interval duration, starting from t_k to t_{k+N}, while DOPF2 runs each time interval. Before executing DOPF1 and DOPF2, the solar irradiance and feeder loading forecasts are assumed to be received by the control room by utilizing historical and field measurement data.

IV. Numerical Results

A. Simulation Setup

In order to validate the performance of the proposed coordination approaches, the IEEE 123-bus test feeder is considered

as a test network with some modifications. PV generation sites are assumed to be installed at the specified buses shown in Fig. 9, where 27 single-phase SIs are connected. Each PV plant is assumed to have an interface to the grid through a SI equipped with a suite of reactive power support functionalities such as $\mathbf{Q}(\mathbf{V})$ and $\mathbf{Q}(\mathbf{\Delta V})$. The PV plants are allowed to be connected in a multi-phase setting with individual SI per phase. The SIs are assumed to be 10% oversized with an active power rating of 100 kW.

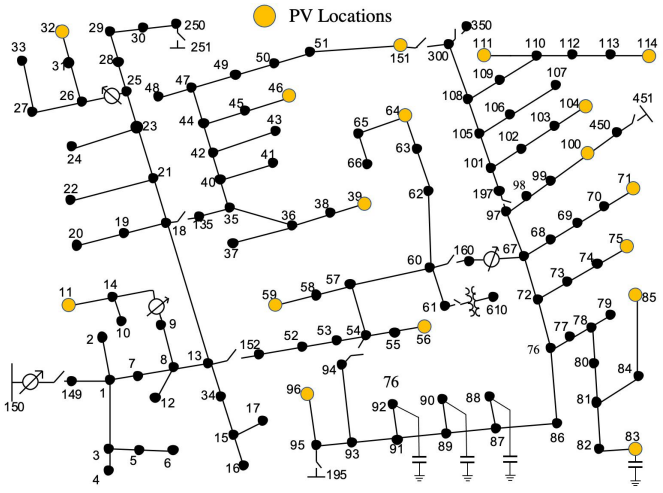

Fig. 9: Modified IEEE 123-Node Feeder.

In addition, all LTCs are considered controllable, and the fixed capacitors are modified as switched capacitors of the same ratings as per the IEEE document. The base loads are converted to constant-PQ type. PV generation profile is generated by scaling the peak power of 120 kW for each PV site. To conduct a daily time-series simulation, the given base load and PV generation capacity are scaled and the aggregated daily active and reactive loading with PV generation capacity profile are shown in Fig. 10.

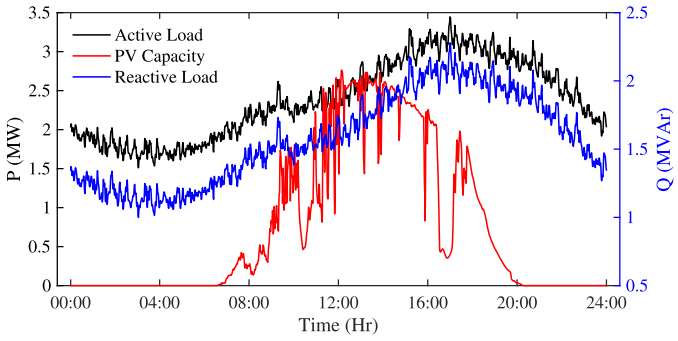

Fig. 10: Aggregated load and PV profiles (1-min resolution).

Table I provides the average daily loading and available PV generation capacity at each phase between hours 10:00 - 14:00. The base PV power is selected such that the PV generation can supply at least 70% of the average loading during peak PV duration.

TABLE I: Per Phase Average Active Loading and PV Generation Capacity Between 10:00 - 14:00 in MW

	Phase-a	Phase-b	Phase-c
Active Load	0.996	0.665	0.807
PV Gen. Cap.	0.713	0.571	0.642

B. Case Studies

Table II summarizes the cases and respective models considered for the two-stage optimization framework for VVC. Case-1 and Case-2 are formed to test the performance of the proposed frameworks under two different Volt-VAr droop functions with common and simplified settings, as shown in Fig. 11. These settings are further combined with the adaptive droop function given in Fig. 12 to enable the adaptive voltage control strategy within the DOPF2 model. Accordingly, in stage-1 optimization, DOPF1 is the model used for all cases, while two variations of DOPF2 are designated in stage 2, where DOPF2-QV is called the Non-Adaptive model while DOPF2-QΔV is the Adaptive.

TABLE II: Considered cases.

Case	Model	Stage-1	Stage-2	Droop Setting
1	Non-Adaptive Adaptive	DOPF1 DOPF1	DOPF2-QV DOPF2-QΔV	Common
2	Non-Adaptive Adaptive	DOPF1 DOPF1	DOPF2-QV DOPF2-QΔV	Simplified

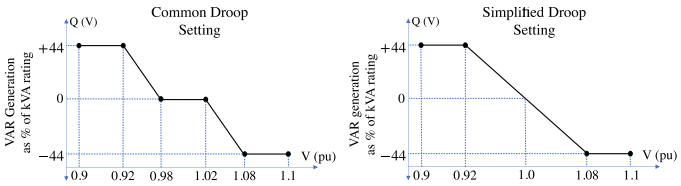

Fig. 11: Volt-VAr droop function settings.

Moreover, to characterize the effect of parameter variations in the Adaptive framework, further investigations are included as sub-cases based on the half-width of linear range in adaptive droop (d) and averaging window length (N_p) used in the adaptive control strategy.

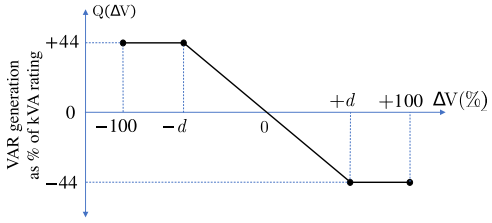

Fig. 12: Adaptive Volt-VAr droop function settings.

Overall, the performance evaluations of the proposed frameworks are presented comparatively through the case studies in terms of the ability to stabilize the PCC voltage profile, whether any additional PV generation curtailment is induced and reactive power support performance depending on the chosen droop function settings.

C. Evaluation of PCC Voltage Response

This section presents the comparative voltage response of each PV generation site connected at PCC under the proposed optimization models. The variability index (VI) is used to assess the level of variations in node voltages in daily operation as follows,

$$VI = \frac{\sigma_v^2}{\mu_v} \times 10^6 \tag{30}$$

where σ_v^2 is the variance and μ_v is the mean of the daily voltage profile of PV connected nodes, the values are scaled by 10^6 for better readability. The higher the value of VI, the more variability is incurred in the daily voltage profile. More intuitively, when the standard deviation (σ_v) gets smaller, the probability of occurrence of inconsistent voltage values becomes reduced, which results in a flatter voltage profile. The variability index calculated at PCC of SIs vary with different model parameters such as averaging window length N_p, and the adaptive Volt-VAr droop width, d of $Q_i(\Delta V_i)$. For N_p, $5/10/15$-sample averaging window lengths are tested with the droop width of $2/4/6/8\%$. Table III summarizes the averaged VI values over all the SI connected nodes for corresponding parameter variations in Case-1 and Case-2, respectively.

TABLE III: Average Variability Index

Case	Adaptive					Non-Adaptive
	Np (min)	$d=2$	$d=4$	$d=6$	$d=8$	
1	5	46.89	48.29	48.94	49.33	51.0
	10	45.39	47.36	48.25	48.78	
	15	44.13	46.59	47.69	48.34	
2	5	36.67	37.45	37.80	38.01	38.86
	10	35.89	36.97	37.46	37.73	
	15	35.26	36.59	37.18	37.52	

According to the obtained VI values, the Adaptive framework continuously achieves less VI value for the Non-Adaptive counterpart in all cases. In Case-1 and Case-2, the least average VI value is observed when the adaptive droop parameter is set to $d = 2$ and averaging window length $Np = 15$ is used. Comparing the average VI values between Case-1 and Case-2, Adaptive framework maintains the least average VI values when using the simplified droop setting.

After the effective parameter characterization based on VI values, comparing the individual voltage profiles can give more visual insights into understanding the performance difference between Adaptive and Non-Adaptive frameworks. To this end, the VI values calculated for each SI-connected node are sorted in descending order, and the highest values are picked for visual inspection. Fig. 13 compares the daily voltage profiles obtained at node $85-c$ in Case-1 and Case-2, respectively. In Case-1, the VI value of 107.5 is obtained with the Non-Adaptive framework, which shows the most considerable variability in the daily voltage profile. In contrast, the Adaptive framework achieves a VI value of 91.43. In Case-2, the Adaptive framework maintains the lowest VI value of 70.88 among all the resulting VI values, including Case-1. As the common simplified droop setting does not have a deadband, it can provide continuous reactive power support in the vicinity of the reference voltage (1 p.u.), which shows an obvious advantage in stabilizing the daily voltage profile.

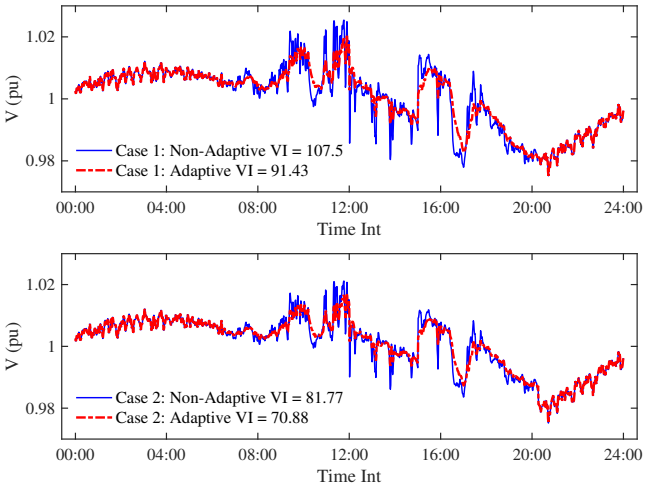

Fig. 13: Daily voltage profile at node $85-c$, $Np = 15, d = 2$.

Even though the Adaptive framework achieves fewer VI values than the Non-Adaptive framework, the PV plant location also has a significant effect on the VI index since the voltage sensitivity varies depending on the electrical distance along the feeder. In [28], authors derive a quantitative measure of bus voltage deviation as a function of power injection deviations of distributed generators and network parameters as follows

$$\Delta V_i^\phi = \sum_{j \in \mathcal{N}^{\text{PV}}} R_{ij}^\phi \Delta P_j^\phi + X_{ij}^\phi \Delta Q_j^\phi, \quad \forall \phi \in \Phi^{\text{PV}} \tag{31}$$

where ΔP_j^ϕ and ΔQ_j^ϕ represent the deviations of power injections from the predicted values. R_{ij}^ϕ and X_{ij}^ϕ denotes the total resistances and reactances of the lines shared by the path from bus i to the substation and the path from bus j to the substation, which is formally expressed as

$$\begin{aligned} R_{ij}^\phi &= \begin{cases} \sum_{(k,l)\in\mathcal{D}^i} r_{kl}^{\phi\phi}, & i = j \\ \sum_{(k,l)\in\mathcal{D}^i\cap\mathcal{D}^j} r_{kl}^{\phi\phi}, & i \neq j \end{cases} \\ X_{ij}^\phi &= \begin{cases} \sum_{(k,l)\in\mathcal{D}^i} x_{kl}^{\phi\phi}, & i = j \\ \sum_{(k,l)\in\mathcal{D}^i\cap\mathcal{D}^j} x_{kl}^{\phi\phi}, & i \neq j \end{cases} \end{aligned}, \phi \in \Phi^{\text{PV}}. \tag{32}$$

$\mathcal{D}^i$ is referred to as the path from node i to the substation, which is comprised of the set of edges that connect a sequence of distinct nodes. Based on these definitions, the voltage volatility at a bus can be concisely described as

$$\mathcal{I}_i^\phi = \sum_{j \in \mathcal{N}^{\text{PV}}} R_{ij}^\phi + X_{ij}^\phi, \quad \forall \phi \in \Phi^{\text{PV}}. \tag{33}$$

The more considerable index value indicates that the node voltage is likely to be more sensitive to the power injection fluctuation incurred in the PV generation.

To investigate and interpret the varying level of voltage fluctuations based on the location of PV plants with respect to the proximity to the substation, the derived voltage volatility index is utilized for the PV plants located at nodes $85-c$ and $11-a$, which the former of these nodes is a remote and the latter is close to the substation. It is found that the volatility index of nodes $85-c$ is $\mathcal{I}_{85}^c = 8.75$ while $\mathcal{I}_{11}^a = 3.34$, which

means the node $85-c$ has more sensitive to the PV injections and larger fluctuations can occur compared to the node $11-a$. It is observed from Fig. 14 that the level of VI index at node $11-a$ is remarkably less compared to that of node $85-c$.

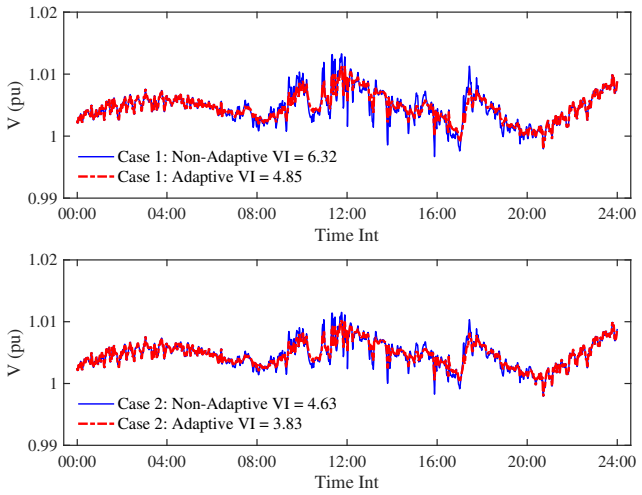

Fig. 14: Daily voltage profile at node $11-a$, $Np=15, d=2$.

D. Comparison of Total Curtailment

Table IV shows the amount of total curtailed active power in the daily operation of SIs corresponding to each test case. The lowest curtailment is achieved in Case-1 as 336.1 kW with the Adaptive framework by setting the adaptive droop width parameter $d = 8\%$ and averaging window length to $Np = 15$ min. However, the Non-Adaptive framework can also maintain a marginally close curtailment level to the Adaptive counterpart by 336.2 kW. It can also be observed that using a common droop setting incurs equal or less curtailment level in general compared to the simplified droop setting in Case-2.

TABLE IV: Total daily PV generation curtailments in kW.

Case	Adaptive					Non-Adaptive
	Np (min)	$d=2$	$d=4$	$d=6$	$d=8$	
1	5	336.4	336.6	336.2	336.3	336.2
	10	336.4	336.3	336.2	336.8	
	15	336.6	336.4	336.5	336.1	
2	5	336.7	336.7	336.6	336.5	336.6
	10	336.4	337.3	336.3	336.4	
	15	337.0	336.3	336.8	336.9	

E. Comparison of Reactive Power Generation

Reactive power support functionality of SIs provides continuous voltage regulation at PCC based on the Volt-VAr droop selected. The Adaptive framework provides continuous reactive power support to both inductive and capacitive regions and can maintain better voltage regulation values compared to the Non-Adaptive framework. Fig. 15 and Fig. 16 show the reactive power support from the SI connected at node $11-a$ and $85-c$ with associated adaptive droop parameters and averaging window length ($Np=5, d=2\%$). It can be observed from the Case-1 of Fig. 15 and Fig. 16 that the Non-Adaptive framework might not always provide reactive power support when the PCC voltage fluctuates within the deadband ($0.98-1.02$ p.u.) of common droop function, which can induce higher VI values as analyzed in the section IV-C. On the other hand, as shown in Case-2, the common simplified droop setting enables continuous reactive power support. The contribution of the adaptive droop within the Adaptive framework can be observed by providing additional reactive power adjustment.

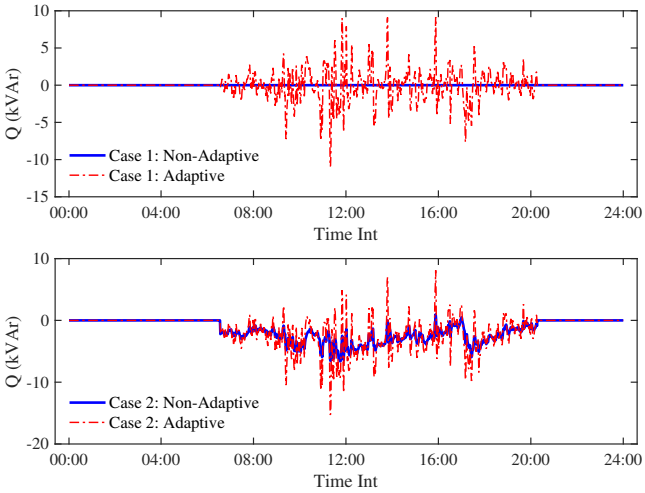

Fig. 15: Reactive power gen. at node $11-a$, $Np=5, d=2$

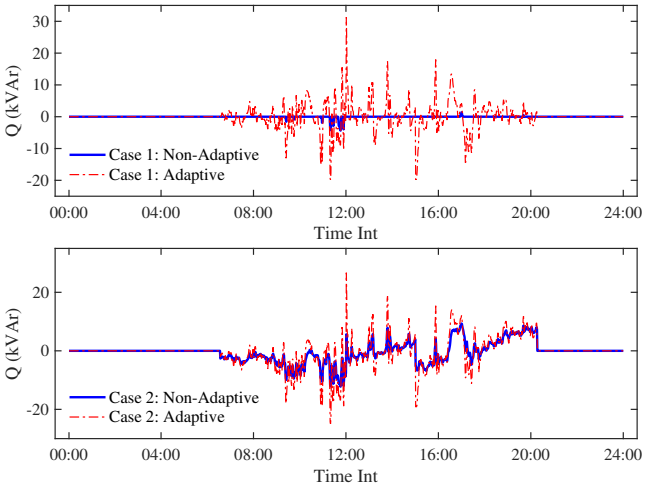

Fig. 16: Reactive power gen. at node $85-c$, $Np=5, d=2$.

F. Dispatch of Legacy Devices

The proposed two-stage framework coordinates the operation of legacy devices through DOPF1 model whose objective function includes the total curtailment ($\mathcal{O}_1$ in p.u.), total voltage deviation ($\mathcal{O}_2$ in p.u.), total number of absolute LTC tap change ($\mathcal{O}_3$) and total absolute CB switching ($\mathcal{O}_4$) terms weighted by $\xi_1, \xi_2, \xi_3, \xi_4$. The degree of significance of each objective can be adjusted by selecting the proper weights. Theoretically, determining the weights can be challenging for problems whose objective terms consist of continuous and

discrete variables. Instead, empirically determining the weights based on the computational tests provides a more practical and effective way. Table V lists a series of computational tests conducted by varying the weights of each objective term corresponding to the objective values obtained.

TABLE V: Effect of weighting on multi-objectives in DOPF1.

ξ_1	ξ_2	ξ_3	ξ_4	$\mathcal{O}_1$	$\mathcal{O}_2$	$\mathcal{O}_3$	$\mathcal{O}_4$	OF_1
1	1	1	1	21.13	238.5	1	0	260.63
1	1	0.1	1	20.51	172.78	46	0	197.89
1	1	0.01	1	20.24	164.45	132	0	186.01
1	1	1	0.1	21.16	210.46	1	18	234.42
1	1	1	0.01	20.36	207.02	1	66	229.04
1	0.1	1	1	20.67	266.1	0	0	47.28
1	0.01	1	1	18.74	335.09	0	0	22.09
0.1	1	1	1	21.16	238.48	1	0	241.59
0.01	1	1	1	21.16	238.48	1	0	239.69
0.01	1	1	1	21.16	238.48	1	0	239.69
10	1	1	1	20.67	241.24	1	0	448.94
100	1	1	1	18.74	305.51	2	6	2,187.51
1000	1	1	1	18.74	305.53	2	6	19,053.53
1	10	1	1	21.06	157.42	34	3	1,632.26
1	100	1	1	20.8	149.98	82	25	15,125.80
1	1000	1	1	20.79	149.82	104	42	149,986.79
1000	1000	1	1	20.19	150.03	116	46	170,382
1000	1000	1000	1000	21.13	238.5	1	0	260,630

It can be observed that there is a tradeoff between the objective terms. Determination of the weights without detailed investigation of individual objective terms may result in unintended LTC and CB switching operations. In this study, DOPF1 is intended to maintain the least number of total switching operations of legacy devices while admitting as much PV power injection as to the grid with an effective voltage positioning strategy. Thus, the most effective weight combination is found by $(1, 0.01, 1, 1)$, resulting in the lowest OF_1.

V. Conclusion

This paper presented two VVC methods for coordinating legacy devices as well as Volt-VAr and adaptive Volt-VAr droop functions of SIs. The devised VVC methods are formulated as a MILP-based DOPF, established on *LinDist3Flow*, and further combined within two-stage optimization frameworks. The first stage optimization runs DOPF1 on a 15-minute timescale, dispatches the tap position of LTCs and on/off status of CBs considering the active power output of SIs. The second stage optimization runs DOPF2 on a 1-minute timescale by utilizing the legacy dispatch decisions from the first stage. It dispatches the SI active and reactive power output considering the advanced voltage regulation support of SIs. The mixed-integer linear mathematical models of LTCs and CBs are incorporated into the first optimization stage. The piece-wise linear models of Volt-VAr and adaptive Volt-VAr droop functions are derived and embedded in the second stage of optimization, which forms two optimization frameworks as adaptive and non-adaptive. In addition, two common Volt-VAr droop settings are investigated in the case studies. The efficiency of the proposed frameworks is comparatively tested on the modified IEEE 123-bus feeder in terms of stabilizing the PCC voltage variability, total incurred active power curtailment, and reactive power support performance of SIs. According to the case studies, the adaptive model outperforms the non-adaptive framework in stabilizing the PCC voltage while maintaining less active power curtailment in daily operation for the investigated parameter variations of the adaptive Volt-VAr droop function. In addition, improved performance is observed when the common simplified droop setting is set within the adaptive framework. Overall, the proposed method provides a complementary and tractable perspective to the VVC study incorporating the advanced Volt-VAr control functions of SIs combining the legacy device operations. Moreover, the proposed frameworks can be incorporated with distributed optimization methods for large systems.

References

[1] J. Romero Aguero and A. Khodaei, "Grid modernization, der integration amp; utility business models - trends amp; challenges," *IEEE Power and Energy Magazine*, vol. 16, no. 2, pp. 112–121, 2018.

[2] "Renewable capacity statistics 2021," *Tech. Report, International Renewable Energy Agency (IRENA), Abu Dhabi*, 2021.

[3] J. Jung, A. Onen, K. Russell, and R. P. Broadwater, "Local steady-state and quasi steady-state impact studies of high photovoltaic generation penetration in power distribution circuits," *Renewable and Sustainable Energy Reviews*, vol. 43, pp. 569–583, 2015.

[4] B. Palmintier, J. Giraldez, K. Gruchalla, P. Gotseff, A. Nagarajan, T. Harris, B. Bugbee, M. Baggu, J. Gantz, and E. Boardman, "Feeder voltage regulation with high-penetration pv using advanced inverters and a distribution management system: A duke energy case study." [Online]. Available: https://www.osti.gov/biblio/1331479

[5] E. Demirok, P. C. González, K. H. B. Frederiksen, D. Sera, P. Rodriguez, and R. Teodorescu, "Local reactive power control methods for overvoltage prevention of distributed solar inverters in low-voltage grids," *IEEE Journal of Photovoltaics*, vol. 1, no. 2, pp. 174–182, 2011.

[6] B. Mirafzal and A. Adib, "On grid-interactive smart inverters: Features and advancements," *IEEE Access*, vol. 8, pp. 160 526–160 536, 2020.

[7] "IEEE standard for interconnection and interoperability of distributed energy resources with associated electric power systems interfaces," *IEEE Std 1547-2018 (Revision of IEEE Std 1547-2003)*, pp. 1–138, 2018.

[8] "IEEE standard conformance test procedures for equipment interconnecting distributed energy resources with electric power systems and associated interfaces," *IEEE Std 1547.1-2020*, pp. 1–282, 2020.

[9] W. H. Kersting, *Distribution system modeling and analysis*. CRC press, 2006.

[10] "Feeder voltage regulation with high-penetration pv using advanced inverters and a distribution management system: A duke energy case study," *Tech. Report, National Renewable Energy Lab. (NREL), USA*, 2016.

[11] F. Ding, Y. Zhang, J. Simpson, A. Bernstein, and S. Vadari, "Optimal energy dispatch of distributed pvs for the next generation of distribution management systems," *IEEE Open Access Journal of Power and Energy*, vol. 7, pp. 287–295, 2020.

[12] K. Turitsyn, P. Šulc, S. Backhaus, and M. Chertkov, "Distributed control of reactive power flow in a radial distribution circuit with high photovoltaic penetration," in *IEEE PES General Meeting*, 2010, pp. 1–6.

[13] Z. Wang, H. Chen, J. Wang, and M. Begovic, "Inverter-less hybrid voltage/var control for distribution circuits with photovoltaic generators," *IEEE Transactions on Smart Grid*, vol. 5, no. 6, pp. 2718–2728, 2014.

[14] M. Noroozian, N. Petersson, B. Thorvaldson, A. Nilsson, and C. Taylor, "Benefits of svc and statcom for electric utility application," in *2003 IEEE PES Transmission and Distribution*

Conference and Exposition (IEEE Cat. No.03CH37495), vol. 3, 2003, pp. 1143–1150 vol.3.
[15] M. Kraiczy, T. Stetz, and M. Braun, "Parallel operation of transformers with on load tap changer and photovoltaic systems with reactive power control," *IEEE Transactions on Smart Grid*, vol. 9, no. 6, pp. 6419–6428, 2018.
[16] A. Singhal, V. Ajjarapu, J. Fuller, and J. Hansen, "Real-time local volt/var control under external disturbances with high pv penetration," *IEEE Transactions on Smart Grid*, vol. 10, no. 4, pp. 3849–3859, 2019.
[17] F. Ding and M. Baggu, "Coordinated use of smart inverters with legacy voltage regulating devices in distribution systems with high distributed pv penetration — increase cvr energy savings," *IEEE Transactions on Smart Grid*, pp. 1–1, 2018.
[18] C. Zhang and Y. Xu, "Hierarchically-coordinated voltage/var control of distribution networks using pv inverters," *IEEE Transactions on Smart Grid*, vol. 11, no. 4, pp. 2942–2953, 2020.
[19] S. Singh, S. Veda, S. P. Singh, R. Jain, and M. Baggu, "Event-driven predictive approach for real-time volt/var control with cvr in solar pv rich active distribution network," *IEEE Transactions on Power Systems*, vol. 36, no. 5, pp. 3849–3864, 2021.
[20] T. M. Aljohani, A. Saad, and O. A. Mohammed, "Two-stage optimization strategy for solving the vvo problem considering high penetration of plug-in electric vehicles to unbalanced distribution networks," *IEEE Transactions on Industry Applications*, vol. 57, no. 4, pp. 3425–3440, 2021.
[21] S. Paudyal, C. A. Cañizares, and K. Bhattacharya, "Optimal Operation of Distribution Feeders in Smart Grids," *IEEE Trans. on Ind. Electron.*, vol. 58, no. 10, pp. 4495–4503, Oct. 2011.
[22] A. Savasci, A. Inaolaji, and S. Paudyal, "Distribution grid optimal power flow integrating volt-var droop of smart inverters," in *2021 IEEE Green Technologies Conference (GreenTech)*, 2021, pp. 54–61.
[23] A. Savasci, A. Inaolaji, and S. Paudyal, "Distribution grid optimal power flow with adaptive volt-var droop of smart inverters," in *2021 IEEE Industry Applications Society Annual Meeting (IAS)*, 2021, pp. 1–8.
[24] M. Rylander, H. Li, J. Smith, and W. Sunderman, "Default volt-var inverter settings to improve distribution system performance," in *Proc. IEEE Power and Energy Society General Meeting*. IEEE, 2016, pp. 1–5.
[25] M. D. Sankur, R. Dobbe, E. Stewart, D. S. Callaway, and D. B. Arnold, "A linearized power flow model for optimization in unbalanced distribution systems," *arXiv preprint arXiv:1606.04492*, 2016.
[26] B. Seal and B. Ealy, "Common functions for smart inverters, 4th edition," *Tech. Report, Electric Power Research Institute (EPRI), Palo Alto, CA*, 2016.
[27] R. A. Jabr, "Linear decision rules for control of reactive power by distributed photovoltaic generators," *IEEE Transactions on Power Systems*, vol. 33, no. 2, pp. 2165–2174, 2018.
[28] Y. Song, Y. Zheng, T. Liu, S. Lei, and D. J. Hill, "A new formulation of distribution network reconfiguration for reducing the voltage volatility induced by distributed generation," *IEEE Transactions on Power Systems*, vol. 35, no. 1, pp. 496–507, 2020.

Alper Savasci (S'19) received the B.S. degree in electrical and electronics engineering from Erciyes University, Kayseri, Turkey, in 2012. He received the M.Sc. degree in electrical engineering from Michigan Technological University, Houghton, MI, USA, in 2018. He is currently pursuing his Ph.D. degree in electrical engineering from Florida International University, Miami, FL, USA. His current research interests are distribution system modeling and optimization.

Adedoyin Inaolaji (S'19) received a B.Eng. degree in Electrical and Electronics Engineering from Covenant University, Ota, Nigeria, in 2014, and an M.S. degree in Electrical Engineering from the Department of Electrical and Computer Engineering, Florida International University (FIU), Miami, FL, USA in 2022, where she is currently working toward the Ph.D. degree in Electrical Engineering. Her research interests include distribution grid modeling, analysis, and optimization techniques.

Sumit Paudyal (S'07, M'12) received the B.E. degree from Tribhuvan University, Nepal in 2003, the M.Sc. degree from the University of Saskatchewan, Saskatoon, Canada, in 2008, and the Ph.D. degree from the University of Waterloo, Waterloo, Canada, in 2012, all in electrical engineering. He was a faculty member at Michigan Technological University, Houghton, MI, USA from 2012 to 2019. Since 2019, he is an Associate Professor in the Department of Electrical and Computer Engineering at Florida International University, Miami, FL, USA. His research interests include distribution grid modeling, dynamic studies, and optimization techniques in power systems.